Dynamics of Charged Colloids in Nonpolar Solvents

Dynamics of Charged Colloids in Nonpolar Solvents

A dissertation presented
by

Tina Lin

to
The Department of Physics
in partial fulfillment of the requirements
for the degree of
Doctor of Philosophy
in the subject of

Physics

Harvard University
Cambridge, Massachusetts
April 2013

Dissertation Advisor: David A. Weitz Tina Lin

Dynamics of Charged Colloids in Nonpolar Solvents

Abstract

Charging is typically not expected in nonpolar environments due to a high electrostatic barrier to charge dissociation. Nevertheless, charge effects are observed in such environments upon the addition of surfactants, which aggregate to form charge-stabilizing reverse micelles. Surfactants facilitate the charging and electrostatic stabilization of particles dispersed in nonpolar solvents. Suspensions of charged particles in nonpolar solvents are found in a variety of applications, such as electrophoretic displays, in which charged pigment particles are arranged with an external electric field to form an image. The ability to precisely control the locations and trajectories of the particles using an electric field is essential. However, the behavior of charged particles in a nonpolar solvent in response to an electric field is not fully understood.

To investigate the behavior of charged particles in nonpolar solvents, we fabricate a novel microfluidic device that allows us to apply an electric field across a particle suspension and directly visualize the particles as they move across a channel. We image the particles, analyze the particle dynamics, and

explore the relationship between the dynamics and the electrical properties of the suspension.

We find that the presence of reverse micelles has a significant effect on particle motion. In a constant applied electric field, the particles initially move, but then unexpectedly slow down and stop. This behavior is due to screening of the applied field by the accumulation of charged reverse micelles at the channel walls. Consequently, the internal electric field within the channel decays exponentially. The decay time constant is dependent on the electrical conductivity of the suspension and the size of the channel. We model this behavior as an equivalent RC circuit.

We also explore the behavior of charged particles in applied fields that are large enough to transport the particles completely across the channel. We find that the transport of particles is governed by a fingering instability. Furthermore, repeated switches of the direction of the field results in the localization of particles into a well-defined, periodic pattern. The wavelength of this pattern is dependent on the frequency of the applied field.

Contents

Citations to previously published work

Chapter 3 has been published as:

"Transport of charged colloids in a nonpolar solvent", T. Lin, T. E. Kodger and D. A. Weitz, Soft Matter, 2013, 9, 5173-5177.

Chapter 1

Introduction

Charge is ubiquitous in polar environments, where charges readily dissociate due to a low electrostatic barrier to ionization. Consequently, charge often plays an important practical role, as, for example, in the electrostatic stabilization of particle dispersions. Electrostatic interactions between the particles are effectively tuned by controlling the salt, and therefore charge, content of the solution. Consider two dissociated monovalent ions in solution: the Coulombic energy of attraction between them is $E = -\frac{e^2}{4\pi\epsilon_r\epsilon_0 d}$, where e is the charge per ion, ϵ_r is the dielectric constant of the solvent, ϵ_0 is the vacuum permittivity, and d is the separation distance. The separation distance at which the Coulombic attraction between the ions equals their thermal energy, kT, is known as the Bjerrum length, λ_B, defined as $\lambda_B = \frac{e^2}{4\pi\epsilon_r\epsilon_0 kT}$, where k is the Boltzmann constant and T is

the absolute temperature. At large separation distances relative to λ_B, the thermal energy of two ions can overcome their Coulombic attraction and charge dissociation is favorable.

The dielectric constant of water, a polar solvent, is $\epsilon \approx 80$; thus, at room temperature, the Bjerrum length is $\lambda_B \approx 0.7$ nm. By contrast, the dielectric constant of a nonpolar solvent is much smaller, $\epsilon \approx 2$; the Bjerrum length is $\lambda_B \approx$ 28 nm. Electrostatic attraction in nonpolar solvents is 40 times greater than in polar solvents. Consequently, charges do not readily dissociate in nonpolar solvents and charge effects are not expected to occur.

Nevertheless, charge has been measured in nonpolar solvents to which certain surfactants have been added: the electrical conductivity of a solution, a measure of the amount of charge, increases with the amount of added surfactant. Clearly, surfactants enable the stabilization of charge in nonpolar solvents. In such solvents, surfactants aggregate to form nanoscale reverse micelles, in which the surfactant molecules are arranged such that their hydrophilic heads compose the core of the reverse micelle and their hydrophobic tails contact the surrounding solvent. These reverse micelles can stabilize charge within their cores and act as charge carriers in nonpolar systems.

For salts in polar solvents, charge originates from the dissociation of salt molecules into oppositely-charged ions: $AB \leftrightarrow A^+ + B^-$. Accordingly, at low concentrations or for weak electrolytes, the electrical conductivity of the solution varies as the square root of the salt concentration. However, for surfactants in nonpolar solvents, the measured electrical conductivity varies linearly with surfactant concentration. This implies that the origin of charge in these systems is not from the dissociation of a surfactant molecule and subsequent stabilization within reverse micelles, but rather from the collision of two uncharged reverse micelles. Upon collision, these reverse micelles exchange ions, resulting in the creation of two oppositely-charged reverse micelles: $2M \leftrightarrow M^+ + M^-$.

The presence of surfactants also facilitates charging and stabilization of particles dispersed in nonpolar media. The charging mechanism in such systems is not fully understood; however, reverse micelles likely play a significant role by stabilizing charges on the particle surface as well as their counter-charges in the bulk solvent. Charged reverse micelles also contribute to screening of particle interactions; thus, similar to electrolytes in polar systems, surfactants can be used to control charge and tune electrostatic interactions in nonpolar particle dispersions. However, the screening lengths are longer and the interactions are stronger in nonpolar systems than in polar systems.

As a consequence of becoming charged, particles obtain an electrokinetic response and can be electrophoretically manipulated with an electric field. The application of an electric field to nonpolar particle dispersions leads to phenomena not typically seen in polar systems. For example, because the amount of charge carriers in relatively low, the timescale and lengthscale of charge screening is increased; then, any movement of charged species, including both the charged reverse micelles and the particles, can result in appreciable charge separation and the subsequent formation of space charge layers. This may lead to significant charge concentration gradients as well as the generation of nonuniform fields within the solution. Additionally, the motion of the charged species in the solution in response to an applied field can generate fluid flow. These effects can contribute to the development of electrohydrodynamic instabilities.

The low electrical conductivity of nonpolar solvents reduces the dissipation of an applied field, electrical current and therefore power consumption, and electrochemical reactions. For these reasons, nonpolar systems are ideal for practical applications; a notable example is electrophoretic displays, in which the ink consists of charged pigment particles, suspended in a nonpolar solvent, and surfactants to stabilize and control charge. The pigment particles are arranged with an electric field to compose a desired image on the display; precise control

over the location and trajectories of the particles is absolutely essential. Electrophoretic display technology was first proposed in the 1970's; however, while conceptually simple, successful commercialization did not occur until recent years. This is in part due to challenges related to charge control and electrohydrodynamic instabilities. While engineering has circumvented some of these problems, a lack of fundamental understanding of these issues remains a key challenge in the continued advancement of electrophoretic display technologies.

Charged particle dispersions are typically characterized by their electrical properties, such as conductivity, electrophoretic mobility, and zeta potential; determining these properties requires the application of an electric field and a measurement of the resulting particle response. For practical applications, it is also important to understand and predict the dynamics of the particles in an electric field and how this particle behavior is related to the electrical properties of the solution. The traditional method of visualizing the particles employs the use of an ITO cell, which consists of a particle solution contained between two large, flat, parallel glass slides that are coated with indium tin oxide (ITO), a transparent, conductive material; these slides act as electrodes through which an electric field is applied to the particle solution. Particle behavior is studied

through observations of pattern formation and optical contrast changes on the electrode surface. However, capturing the trajectories of the particles as they are transported between electrodes demands a new method of visualization. We construct a novel microfluidic device that allows us to apply an electric field across a particle solution and directly visualize the plane of the electric field lines and particle motion; thus, we are able to capture the full range of particle motion in real-time. This device, along with methods used to study charged particle dispersions, is described in **chapter 2**.

In **chapter 3**, we investigate the transport of charged colloidal particles suspended in a nonpolar solvent by visualizing their motion across a channel in response to an applied electric field. We find that the presence of reverse micelles has a significant effect on particle motion: in a constant field, the particles initially move, but then unexpectedly slow down and stop. This behavior is due to screening of the applied field by the accumulation of charged reverse micelles at the channel walls; consequently, the internal electric field decays exponentially. The time constant of decay depends on the electrical conductivity of the particle dispersion and the width of the channel. We model this behavior as an equivalent RC circuit and compare it to an electrochemical cell.

In **chapter 4**, we explore the dynamic behavior of charged particles in applied electric fields that are large enough to transport the particles completely across the channel. We find that the transport of particles is governed by a fingering instability. We compare this fingering instability with the well-known Rayleigh-Taylor instability. Furthermore, we find that repeated switches in the direction of the applied field results in the localization of particles into a well-defined, periodic pattern. Particle diffusion during the time between switches is critical in determining whether this pattern forms. The characteristic wavelength of the pattern is dependent on the frequency of the applied field.

In **chapter 5**, we explore the capabilities of our microfluidic device for further studies of charged particle suspensions in nonpolar solvents. We also discuss the implications of our results for practical applications, particularly electrophoretic displays.

Chapter 2

Experimental methods

2.1 Microfluidic device

We fabricate a microfluidic device that enables us to visualize particle motion as we apply an electric field across the particle suspension. The device consists of three parallel channels. The outer two channels are filled with a low-temperature solder, forming two parallel electrodes. A particle suspension is injected into the center channel. A top-view image of the device and an image of a suspension of charged PMMA (polymethyl methacrylate) particles within the device are shown in Figure 2.1. Typically, the center channel is 20 – 500 µm wide, the outer channels are 100 µm wide, the walls separating the channels are 10 µm wide, and all the channels are 25 – 50 µm high.

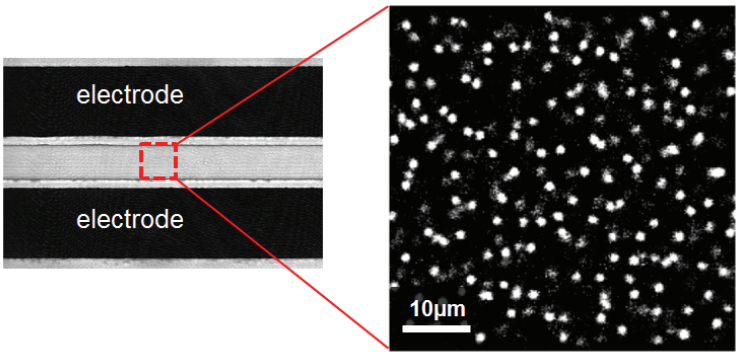

Figure 2.1: Left: A top-view image of the microfluidic device. Two electrodes are parallel to a central channel which can be filled with a particle suspension. Right: Image of 1-μm PMMA particles suspended in decalin, with 10 mM AOT (Aerosol OT), within the channel, obtained using a confocal microscope.

Because the commonly-used PDMS (polydimethylsiloxane) is susceptible to swelling by organic solvents, we instead use Norland Optical Adhesive (NOA 81) as the material for our devices. The NOA is more resistant to swelling by organic solvents. Fabrication of NOA devices follows the same general photolithography protocol as for PDMS devices, but with a few notable differences, which are described below.

- The printed mask is of opposite polarity, resulting in an SU-8 master which is the complement of what is typical for conventional PDMS devices. This SU-8 master is used to mold a PDMS master, which is then used to mold the channels of the NOA device on a glass substrate.
- A second PDMS master consists of posts corresponding to the inlets and outlets of the NOA device.

- The NOA channels and the thin NOA slab, with inlet and outlet holes, are aligned and bonded together.
- Fabrication of and connections to the electrodes require an additional PDMS layer on top of the NOA device. The PDMS layer has holes punched through it to allow access the inlets and outlets of the appropriate channels. This layer is bonded to the NOA after plasma treatment.

2.2 Visualization

We capture images of the particles as they move in response to an applied electric field. We use either a high-speed camera (Phantom V7) or a confocal microscope (Leica). We analyze the images and track the locations of particles using MATLAB.

Chapter 3

Transport of charged colloids in a nonpolar solvent

3.1 Introduction

Polar environments have a low electrostatic barrier to charge dissociation; consequently, charge is ubiquitous and often plays an important practical role, as, for example, in the stabilization of colloidal dispersions. Electrostatic interactions in these dispersions are readily tuned through addition of salt [1]. By contrast, in nonpolar solvents, charges do not readily dissociate and charge-induced effects are typically not expected. Nevertheless, charge-induced effects are made possible through the addition of surfactants [2-5]: In nonpolar solvents, surfactants aggregate to form reverse micelles, which can stabilize charge within

their cores. Thus, reverse micelles solubilize charge, allowing for dissociation of charge from the surface of colloidal particles as well as stabilization of charge on the surface of the particles [3-12]. This provides a mechanism to charge-stabilize colloidal suspensions in nonpolar environments that is very similar to that of polar environments. Particle suspensions charged with reverse-micelle-forming surfactants are central to a variety of applications [12,13], including electrophoretic displays, in which charged pigment particles are driven by an electric field to compose an image [14]. In such applications, the ability to precisely control the trajectories and locations of charged particles with an electric field is essential. However, the electrical properties of charged particle suspensions are influenced by the reverse micelles in the bulk fluid [15], which not only stabilize the counter-charges but also stabilize additional charges, resulting in increased electrical conductivity and charge screening. Thus, reverse micelles can have an effect on the response of charged colloidal particles to an applied electric field [16]; however, the details of this scenario are not fully understood. Such knowledge is important for practical purposes, including the ability to predict and control charged particle behavior; it is also essential for gaining a better understanding of the electrodynamic properties of such systems. This

requires a detailed investigation of charged particle motion in nonpolar solvents and the influence of reverse micelles on this motion.

Here, we investigate the dynamics of colloidal particles suspended in a nonpolar solvent and charged through the addition of reverse micelles by directly visualizing their motion across a microfluidic channel in response to an applied electric field. We find that the presence of the charged reverse micelles has a significant effect on particle transport: In a constant applied electric field, the colloidal particles initially move, but then unexpectedly slow down and stop. We show that this transport behavior is due to a buildup of charged reverse micelles, which subsequently screen the applied field. As a result, the internal electric field within the channel decays exponentially in time; the decay behavior depends on the conductivity of the suspension and the size of the channel. This system is modeled as an equivalent RC circuit.

3.2 Experimental

We synthesize 1 μm diameter, fluorescently-labeled poly(methyl methacrylate) (PMMA) colloidal particles [17]. Methyl methacrylate and methacrylic acid monomers, dimethylacrylate-polydimethylsiloxane stabilizer Gelest DMS-R31, BODIPY 543 fluorophore, AIBN initiator, and hexane solvent are placed in a

flask and heated to 80℃ under reflux for 6 hours. The particles are cleaned and resuspended in decalin at a volume fraction of 0.1%. The presence of methacrylic acid in the polymer particle allows for a negatively-charged ionizable group. The particles also have polydimethylsiloxane (PDMS) brushes on their surfaces which provide steric stabilization.

We use aerosol-OT (AOT, or sodium di-2-ethylhexylsulfosuccinate) as the charge control agent in our particle suspensions; AOT is a surfactant with a polar head and two nonpolar hydrocarbon tails. In nonpolar solvents, AOT forms reverse micelles with a radius on the order of 1 nm. A fraction of the AOT reverse micelles are charged; these typically contain a single charge. Even though the reverse micelles have less charge than the particles, they are much smaller in size; therefore, the mobility of charged reverse micelles is typically at least an order of magnitude larger than that of the charged particles.

After adding AOT to a particle suspension, we allow the suspension to equilibrate for at least 1 day and sonicate it to ensure a homogeneous dispersion. The conductivity of the particle suspensions is measured with a Scientifica 627 conductivity meter.

To investigate the motion of the particles, we use a microfluidic device that allows us to apply an electric field across the particle suspension and directly

observe the most important dimension: the plane consisting of the field lines and particle motion. The microfluidic device is fabricated with Norland Optical Adhesive (NOA 81) [18]. The device consists of three parallel channels which are separated by a 10 µm-wide wall and all of the channels are 25-µm-high. The two outer channels are filled with a low-temperature solder (Indium Corporation), forming two parallel electrodes, as shown in Figure 3.1. The width of each of the electrodes is 100 µm, while the width of the central channel is varied for different devices. The central channel is filled with the particle suspension, and then sealed with epoxy.

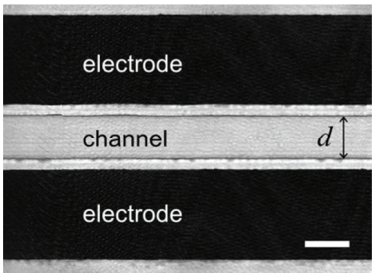

Figure 3.1: Microfluidic device consisting of a channel of width d and two parallel electrodes. A thin wall separates each electrode from the channel. The scale bar is 50 µm.

The electrodes are connected in series to a function generator (Agilent 33250A) and a high-voltage amplifier (Trek 2210). We apply and repeatedly reverse a voltage difference across the particle suspension; as a result, the charged particles move back and forth across the channel. We image the particles using a

confocal microscope (Leica SP5). As the particles move in response to a reversal in the applied field, we capture sequential images at rates of up to 200 frames per second; these images are used to track the locations of the particles. We wait several seconds between each reversal; this allows us to capture the full range of particle motion, as most of the motion occurs within a timeframe on the order of 10 - 100 ms.

3.3 Results and Discussion

We visualize a particle suspension without any AOT within a 50-µm-wide channel: in response to an applied constant voltage of 10 V, the particles move towards the negative electrode, indicating that they are positively charged. The particles move until they contact the channel wall, whereupon they remain stationary. When the polarity of the applied field is reversed, the particles move in the opposite direction as they did before; they are transported completely across the channel until they reach the opposite wall, whereupon they again remain stationary. Particle motion is primarily in the direction perpendicular to the electrodes, along the electric field lines; additionally, the particles appear to move at a constant velocity across the channel. Images of particle transport are shown in Figure 3.2(a). That these particles are charged even in the absence of

any added charge control agent is surprising. Moreover, based on the particle synthesis procedure, the sign of the charge on these particles is unexpected. It is possible that the source of charge is due to trace contaminants; however, this charging behavior is reproducible.

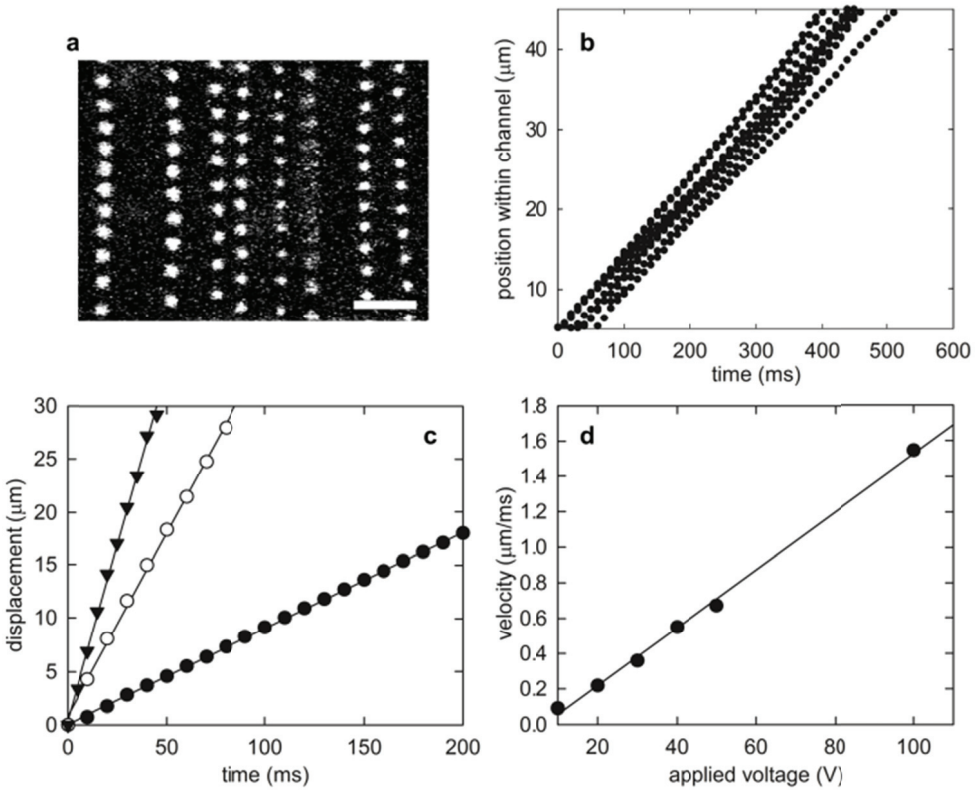

Figure 3.2: Transport of particles with no AOT across a channel of width $d = 50$ µm in response to a reversal in the applied voltage. (a) 15 superimposed consecutive images of particles moving across an area within the channel; the applied voltage is 10 V. The electrodes are located above and below the pictured area; the particles move from top to bottom. The time between each image is 18 ms. The scale bar is 10 µm. (b) Particle locations along the direction of the applied field; the applied voltage is 10 V. (c) Average particle displacements and linear fits for different applied voltages: 10 V (filled circles), 30 V (open circles), and 50 V (triangles). (d) Average particle velocity as a function of applied voltage; the line is a linear fit.

To further analyze the motion of these particles, we track each individual particle as it moves across the channel after the polarity of the applied field is reversed. We focus on the primary direction of motion: in the direction of the applied field. Particle trajectories along this direction are linear in time, as shown in Figure 3.2(b); this indicates that the velocity of each particle as it travels across the channel is indeed constant. For different applied voltages, we measure the individual particle trajectories and average them: the particles move across the channel faster as the voltage is increased, as shown in Figure 3.2(c). The particle velocity, v, is obtained from the slope of the linear fit of the average particle trajectory; it increases linearly with the applied voltage as shown in Figure 3.2(d). Since the applied field, E_A, is the applied voltage divided by the distance between electrodes, we can determine the electrophoretic mobility, μ, from $v = \mu E_A$; we find that $\mu = 9.73 \times 10^{-10}$ m^2/Vs. By assuming that particle charge, Q, is related to mobility by $Q = 6\pi\eta\mu a$, where η is the liquid viscosity and a is the particle radius, we find that these particles have about 170 elementary charges.

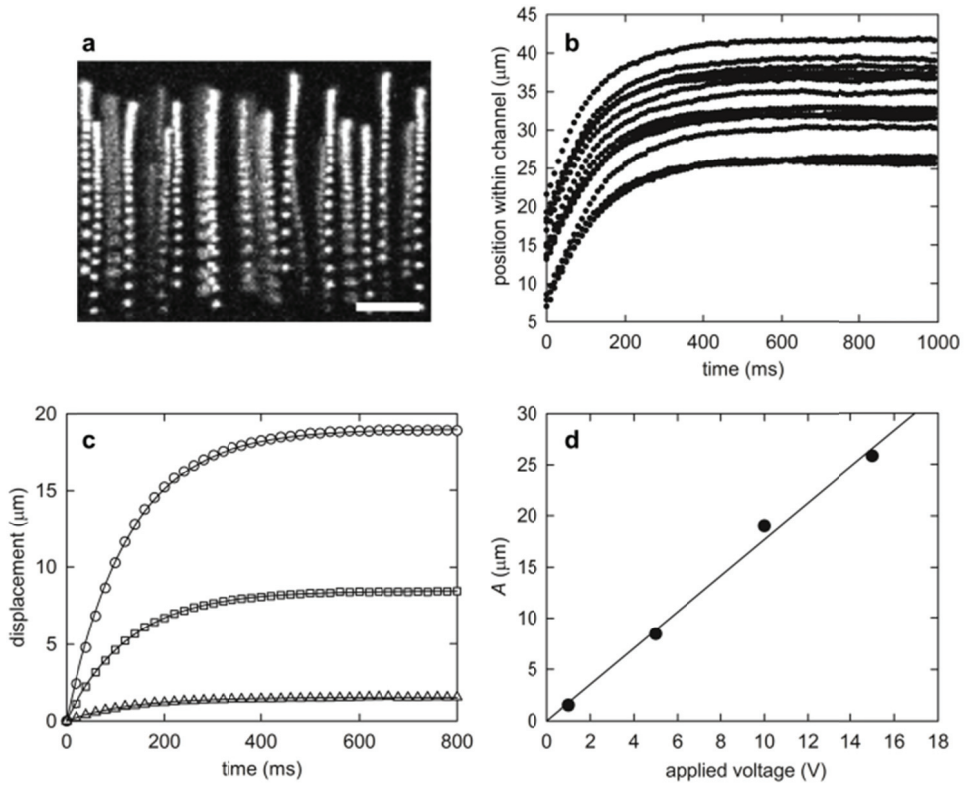

Figure 3.3: Transport of particles with 10 mM AOT across a channel of width d = 50 μm in response to a reversal in the applied voltage. (a) 30 superimposed consecutive images of particles moving within the channel when the applied voltage of 10 V is reversed. The electrodes are located above and below the pictured area; the particles move from bottom to top. The time between each image is 18 ms. The scale bar is 10 μm. (b) Particle locations along the direction of the applied field; the applied voltage of 10 V is reversed at time $t = 0$. (c) Average particle displacements for different applied voltages: 10 V (circles), 5 V (squares), 1 V (triangles). The solid lines are fits to the exponential function $A(1 - \exp(-t/\tau))$. (d) The total distance traveled by the particles, A, as a function of the applied voltage; the solid line is a linear fit.

When we add AOT to the solution, hence adding additional charges, we observe drastically different behavior. In response to a reversal of the applied

constant voltage of 10 V, the particles in the suspension, to which we have added 10 mM AOT, initially move along the direction of the applied field, but then slow down and stop before arriving at the channel wall. Despite the continuously applied voltage, the particles no longer accumulate at the channel wall. When the polarity of the applied field is reversed, the particles move in the opposite direction, but then again slow down and stop before they contact the wall; images of particle transport are shown in Figure 3.3(a). The measured trajectories of these particles along the direction of the applied field are nonlinear in time, as shown in Figure 3.3(b). Furthermore, the initial movement of these particles is towards the positive electrode, indicating that the charge has reversed and they are now negatively charged. We had previously found that, without AOT, the particles are positively charged; similar charge sign reversal upon the addition of charge control agents has also been observed with other nonpolar particle systems [9].

The nonlinear transport behavior is observed over a range of applied voltages, as shown in Figure 3.3(c). We apply voltages that are large enough to induce visually discernable particle motion, yet small enough such that the particles do not reach the channel wall; this enables us to track the full range of particle motion. While the particles always move, slow down, and then stop, the distance

they travel is dependent on the applied voltage. To quantify this behavior, we fit the average particle trajectories to an exponential function, $A(1 - \exp(-t/\tau))$, where the magnitude, A, corresponds to the distance traveled by the particles and the time constant, τ, corresponds to the decay of particle motion in time. We find that A grows linearly as a function of applied voltage, as shown in Figure 3.3(d). By contrast, τ does not change with voltage; this is shown in Figure 3.4(a).

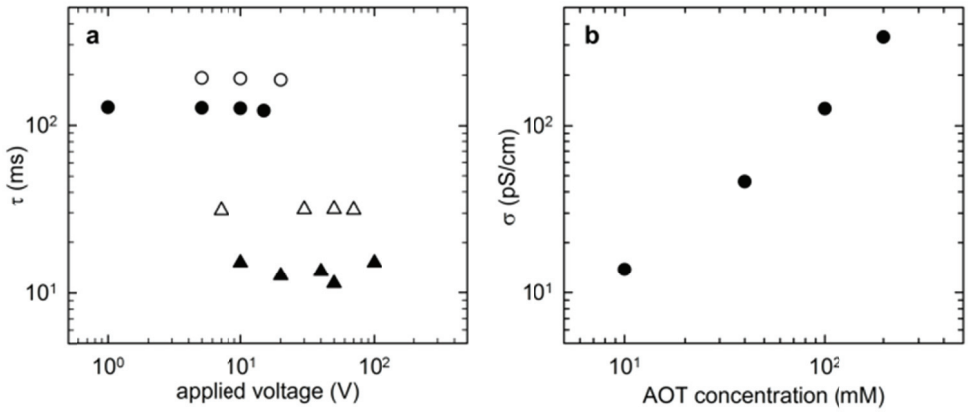

Figure 3.4: (a) Time constants, τ, of decay of particle motion at different applied voltages for different AOT concentrations: 10 mM (circles) and 100 mM (triangles), and different channel widths: 50 µm (filled symbols) and 100 µm (open symbols). The time constant is independent of applied voltage. (b) Conductivity, σ, of the particle suspension versus AOT concentration. The dependence is roughly linear.

We observe similar particle behavior as we vary the AOT concentration, or as we vary the channel widths; in an applied constant voltage, the particle motion

decays in time. The decay time constant does not depend on the applied voltage; however, τ decreases as the AOT concentration is increased and τ increases with channel width, as shown in Figure 3.4(a). In general, larger voltages are required for larger AOT concentrations; this may be in part due to the increase in the amount of charged species in the solution when AOT is added. To determine the amount of charged species, we measure the electrical conductivity of the particle suspension; it increases approximately linearly with AOT concentration, as shown in Figure 3.4(b). Clearly, the motion of particles with AOT differs significantly from the motion of particles without AOT; thus, the reverse micelles must play an important role. When a constant field is applied across the channel, the charged particles and the charged reverse micelles move in response. The charged reverse micelles have a higher mobility than the particles; thus, they travel faster through the fluid and arrive at the channel walls sooner. The positively and negatively charged reverse micelles accumulate at opposite channel walls. These reverse micelles induce an electric field across the channel in the direction opposite to that of the applied field; consequently, the internal electric field, which is the superposition of the applied field and the induced field, is decreased. As a result, the charged species in the bulk slow down. Eventually, the buildup of

charged reverse micelles is sufficiently large enough to completely neutralize the applied field; at this point, the colloidal particles stop moving entirely.

To determine how the internal electric field is affected by the charged reverse micelles, we consider the rate of their accumulation at the channel walls. The current density within the bulk, j, is given by $j = \sigma E^*$, where σ is the suspension conductivity and E^* is the internal field. The internal field is initially equal to the applied field, E_A. From the current density, we determine the rate of accumulation of charge per unit area, q, at either wall: $\mathrm{d}q/\mathrm{d}t = j = \sigma E^*$. The field induced by the accumulated reverse micelles, E_m, reduces the internal field: $E^* = E_A - E_m$. The applied field is held constant; therefore, the change in the internal field is $\mathrm{d}E^*/\mathrm{d}t = -\mathrm{d}E_m/\mathrm{d}t = -\frac{1}{d}\mathrm{d}V_m/\mathrm{d}t$, where V_m is the total voltage drop across the accumulated reverse micelles at both walls and d is the width of the channel. Since V_m is proportional to the amount of charge accumulated at the walls, $\mathrm{d}E^*/\mathrm{d}t \sim -\frac{1}{d}\sigma E^*$. The solution to this expression is $E^* = E_0 \exp(-t/\tau)$, where E_0 is E^* at $t = 0$ and $\tau \sim (d/\sigma)$ is the decay time constant. The exponential form of this internal field is consistent with the observed particle motion.

We also predict that τ is independent of the applied field; this is consistent with our observations of particle motion. In addition, we explicitly predict that τ

$\sim (d/\sigma)$. To test this prediction, we measure the average τ over the applied voltages as we vary the channel width and suspension conductivity. We indeed find that the average time constant varies linearly with d/σ, as shown in Figure 3.5. This confirms our prediction and supports our picture that the decay of the internal electric field is due to the accumulation of charged reverse micelles.

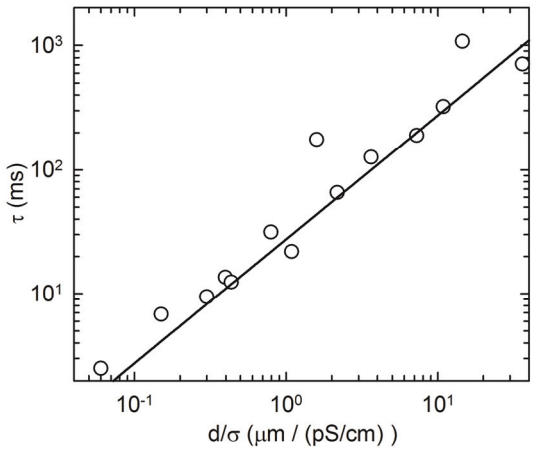

Figure 3.5: Decay time constant as a function of d/σ. The line is a linear fit.

The accumulation of charge at an electrode upon application of an external field is reminiscent of an electrochemical cell. This can be modeled as an RC circuit [15,19,20]: The equivalent circuit consists of a resistor, the suspension, connected in series with two capacitors, the two interfaces. In an electrochemical cell, the resistance is $R = d/\sigma$ and the capacitance of each interface is $C = \varepsilon/\lambda$, where ε is the dielectric constant of the solution and λ is the Debye screening length. The total capacitance for the two interfaces in series is $C/2$. The

screening length scales as $\sigma^{-1/2}$ [4]; thus, the RC time constant is $\tau = \frac{d}{\sigma}\frac{\varepsilon}{2\lambda} \sim \frac{d}{\sqrt{\sigma}}$. By contrast, our measurement shows that time constant scales as (d/σ). To explain this behavior, we consider the details of our microfluidic device: There is a wall of NOA separating each metallic electrode from the electrolyte; to account for these walls, the capacitance of each interface becomes $\frac{\varepsilon}{(\lambda+w)}$, where $w = 10$ μm is the width of the wall. The typical value of λ in nonpolar systems is on the order of 100 nm - 1 μm, at least an order of magnitude smaller than w; therefore, the capacitance is dominated by the wall thickness, and is a constant. The resultant time constant thus varies as (d/σ), in direct agreement with our measurements.

After the reverse micelles have completely screened the applied field and the particles have stopped moving, the internal field is $E^* = E_A - E_m = 0$. At this point, the field induced by the reverse micelles is equal in magnitude to the applied field, $E_m = E_A$, but in the opposite direction. When the applied field is reversed, it is then in the same direction as the induced field; at this point, the magnitude of the internal field is actually twice that of the applied field: $E^* = E_A + E_m = 2E_A$. Therefore, the particles travel twice as fast and twice as far compared to how they would if the field was turned on from 0. Similarly, if the applied field is turned off after complete screening, going from E_A to 0, the field

induced by the micelles still remains: $E^* = -E_A$. Thus, the particle motion when the field is turned off is the same but in the opposite direction as when the field is turned on. We observe such particle behavior when the field is turned on, reversed, and then turned off, as shown in Figure 3.6; in addition to causing the decay in particle motion in a constant field, the accumulated reverse micelles have a major effect on the particle motion when the applied field is then changed. This behavior is relevant for electrophoretic displays, in which the applied electric field is frequently and repeatedly reversed as well as turned on and off; the image quality must be maintained through these changes in the applied field.

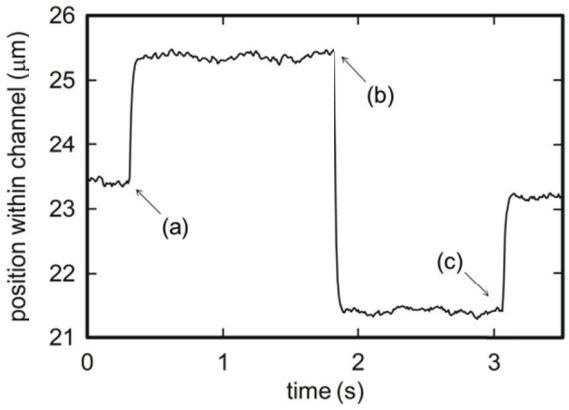

Figure 3.6: Average particle trajectory when the applied voltage is (a) turned on from 0 to 30 V, (b) reversed, then (c) turned off to 0 V. The AOT concentration is 40 mM and d is 50 μm.

3.4 Conclusion

Here, we find that the presence of charged AOT reverse micelles has a significant effect on the transport of charged particles in a nonpolar solvent. Through direct visualization of the motion of the charged particles, we are able to probe the internal electric field across the suspension. Despite a constant applied electric field, the internal electric field decays exponentially in time; this is due to the accumulation of charged AOT reverse micelles at the channel walls which screens the applied field. This does not occur for particle suspensions without any AOT because the relatively low amount of charge in the solution is too small to significantly affect the internal field. The screening effect poses an important challenge for electrophoretic display technology, as surfactants similar to AOT are commonly used to stabilize charge in nonpolar particle dispersions. Our investigation of the dynamics of charged particles in a nonpolar solvent in an applied electric field provides a basis for the further investigation of methods to eliminate or overcome any undesired effects of charged reverse micelles on charged particle transport.

References

[1] E. R. Russell, J. Sprakel, T. E. Kodger and D. A. Weitz, Soft Matter, 2012, 8, 8697.

[2] Q. Guo, V. Singh and S. H. Behrens, Langmuir, 2010, 26, 3203.

[3] I. D. Morrison, Colloids Surf., A, 1993, 71, 1.

[4] M. F. Hsu, E. R. Dufresne and D. A. Weitz, Langmuir, 2005, 21, 4881.

[5] S. K. Sainis, J. W. Merrill and E. R. Dufresne, Langmuir, 2008, 24, 13334.

[6] C. E. Espinosa, Q. Guo, V. Singh and S. H. Behrens, Langmuir, 2010, 26, 16941.

[7] Q. Guo, J. Lee, V. Singh and S. H. Behrens, J. Colloid Interface Sci., 2013, 392, 83.

[8] G. S. Roberts, R. Sanchez, R. Kemp, T. Wood and P. Bartlett, Langmuir, 2008, 24, 6530.

[9] G. N. Smith and J. Eastoe, Phys. Chem. Chem. Phys., 2013, 15, 424.

[10] S. M. Hashmi and A. Firoozabadi, Soft Matter, 2012, 8, 1878.

[11] J. W. Merrill, S. K. Sainis and E. R. Dufresne, Phys. Rev. Lett., 2009, 103, 138301.

[12] K. E. Tettey, M. Q. Yee and D. Lee, Langmuir, 2010, 26, 9974.

[13] V. Novotny, Colloids Surf., 1987, 24, 361.

[14] B. Comiskey, J. D. Albert, H. Yoshizawa and J. Jacobson, Nature, 1998, 394, 253.

[15] M. Karvar, F. Strubbe, F. Beunis, R. Kemp, A. Smith, M. Goulding and K. Neyts, Langmuir, 2011, 27, 10386.

[16] F. Strubbe, F. Beunis, M. Marescaux, B. Verboven and K. Neyts, Appl. Phys. Lett., 2008, 93, 254106.

[17] S. M. Klein, V. N. Manoharan, D. J. Pine and F. F. Lange, Colloid Polym. Sci., 2003, 282, 7.

[18] D. Bartolo, G. Degre, P. Nghe and V. Studer, Lab Chip, 2007, 8, 274.

[19] M. Z. Bazant, K. Thornton and A. Ajdari, Phys. Rev. E: Stat., Nonlinear, Soft Matter Phys., 2004, 70, 021506.

[20] D. C. Prieve, J. D. Hoggard, R. Fu, P. J. Sides and R. Bethea, Langmuir, 2008, 24, 1120.

Chapter 4

Pattern formation of charged particles in an electric field

4.1 Introduction

In nonpolar solvents, charge dissociation is energetically unfavorable; thus, charge stabilization and charge-induced effects are typically expected to be insignificant. Nevertheless, charge can be stabilized in nonpolar solvents upon the addition of suitable surfactants [1-4], thereby providing a mechanism to charge and electrostatically stabilize particle dispersions [2-11]. This effect is utilized in a variety of applications [11,12]; for example, in electrophoretic displays, the charging of pigment particles in a nonpolar solvent enables them to be transported by an externally-applied electric field to form an image [13].

However, achieving the requisite level of control over the movement and locations of charged particles using an electric field is still a major challenge. Upon application of an electric field, particles in an initially homogeneous dispersion commonly form patterns composed of ordered structures or clusters on the electrode surface [14-17]; this behavior degrades the performance of electrophoretic displays by limiting image contrast and resolution. Such patterns can be modified or even eliminated by tuning the strength and frequency of the applied field, the confinement geometry, and the chemical and charge properties of the particle suspension; however, the origin of these patterns remains unclear. The formation of patterns is often attributed to complex particle dynamics that result from the interplay between electrokinetic and hydrodynamic effects, in which field-induced electrohydrodynamic flow ultimately leads to the aggregation of the particles into pattern-forming structures [18]. Typically, the particles that compose these patterns are visualized after they are deposited on a transparent, planar electrode surface [16,17]; the dynamics of pattern formation are never directly observed. Direct visualization of particle motion through the fluid would help elucidate the relationship between particle dynamics and pattern formation; such knowledge is essential for fully understanding the response of charged particles in nonpolar solvents to an applied electric field.

Here, we investigate the dynamics of charged particles in a nonpolar solvent in response to an applied electric field. We use a microfluidic device that allows us to apply an electric field across a suspension of carbon black particles confined within a channel; by combining this device with high-speed imaging, we directly monitor the full motion of the charged particles. Upon being repeatedly driven back and forth across the channel by an alternating electric field, the particles indeed form a well-defined pattern. This pattern results from an instability that occurs during particle transport across the channel in which the rapidly advancing particle front develops fingers. The characteristic wavelength of the pattern is dependent on the frequency at which the applied field is switched.

4.2 Experimental

We use a suspension of 0.5 wt. % carbon black particles dispersed in Isopar G, a nonpolar solvent. To solubilize charge in the solution, 0.5 wt. % surfactant is added as a charge control agent. The surfactant increases the conductivity of the solution to 15000 pS/m; this is more than four orders of magnitude higher than the conductivity of pure Isopar G. The carbon black particles have a characteristic size of 140 nm; their surfaces are chemically modified with polymer brushes that are 3 – 5 nm to be positively charged when the charge control agent

is added. We fabricate a microfluidic device that allows us to observe the motion of the particles within a microfluidic channel in response to an electric field applied across this channel. The device is fabricated from Norland Optical Adhesive (NOA81) [19] and consists of three parallel channels: the center channel is 50 μm wide and the two outer channels are 100 μm wide; all of the channels are 25 μm high. These channels are separated by a wall that is 10 μm wide. The outer channels are filled with a low-temperature solder (Indium Corporation); these form two parallel electrodes through which we can apply an electric field across the center channel. A cross-sectional schematic of the device is shown in Figure 4.1(a). To ensure a homogeneous dispersion, we sonicate the particle suspension. The suspension is injected into the center channel of the device. This channel is then sealed with epoxy. The electrodes are connected in series to a function generator (Agilent 33250A) and a high-voltage amplifier (Trek 2210). Particle motion is imaged with a high-speed camera (Phantom V7) at frame rates of up to 10 kHz with a resolution of 800 × 200 pixels.

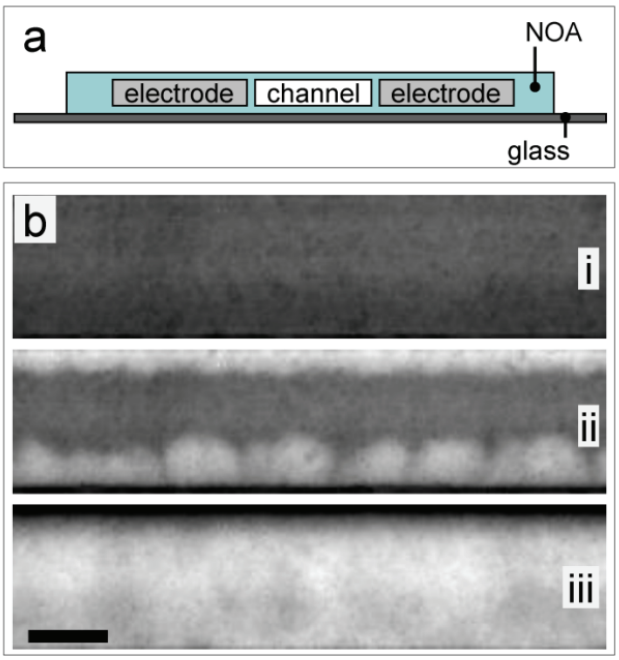

Figure 4.1: (a) Cross-sectional schematic of microfluidic device. (b) Top view of a channel containing carbon black particles. The particles are initially distributed homogenously within the channel in the absence of an applied field (i), partially transported to the bottom wall when a field of magnitude 2 V/μm is first applied across the channel (ii), and completely packed at the top wall when the direction of the field is switched (iii). The particles are transported completely across the channel and packed at the wall after all subsequent switches. Scale bar is 25 μm.

4.3 Results and Discussion

In the absence of an applied electric field, the particles diffuse freely within the channel and are homogeneously distributed, as shown in Figure 4.1(b)(i). When an external field with a magnitude of 2 V/μm is applied for the first time, the particles are transported towards the negative electrode. Most of the particles are packed against the wall; however, a small subpopulation of particles remains

in the central region of the microfluidic channel, as shown in Figure 4.1(b)(ii). When the direction of the field is switched, all of the particles are transported completely across the channel and pack at the opposite wall; this time, in contrast with the initial application of the field, very few particles remain in the bulk, as shown in Figure 4.1(b)(iii). Thus, a switch in the applied field has a stronger effect on the particles than the initial application of the field. This is likely due to charges in the solution that have been separated by the applied field; these separated charges induce an additional field which contributes to driving particle motion when the applied field is switched [20]. In all subsequent switches, all the particles are transported across the entire channel and are packed at the opposite channel wall.

We periodically alternate the applied field and thereby drive the particles back and forth between the channel walls. The time between consecutive switches, t_s, is 1 s. To probe the full details of particle motion, we acquire a sequence of images as the particles are transported across the channel in response to a switch. Initially, the particles are packed homogeneously at the wall. When the field is switched, the particles do not all move simultaneously across the channel; instead of remaining uniform, the particle front develops finger-shaped protrusions that grow longer as the front advances, as shown in the left panel of

Figure 4.2. All of the particles are packed at the opposite wall within 50 ms of the switch. The change in the shape of the particle front from being initially flat to developing fingers during transport occurs for every subsequent switch in the applied field. By contrast, dramatically different behavior occurs when t_s is increased to 5 s. After several switches, the particles are no longer packed homogeneously at the wall following each switch; instead, they become localized in a well-defined, periodic pattern along the wall. The particles in each localized region of higher concentration form plume-like structures as they are transported across the channel, as shown in the right panel of Figure 4.2; the particles deposit on the opposite wall at locations corresponding to these plumes. Thus, the pattern is maintained through continued switches.

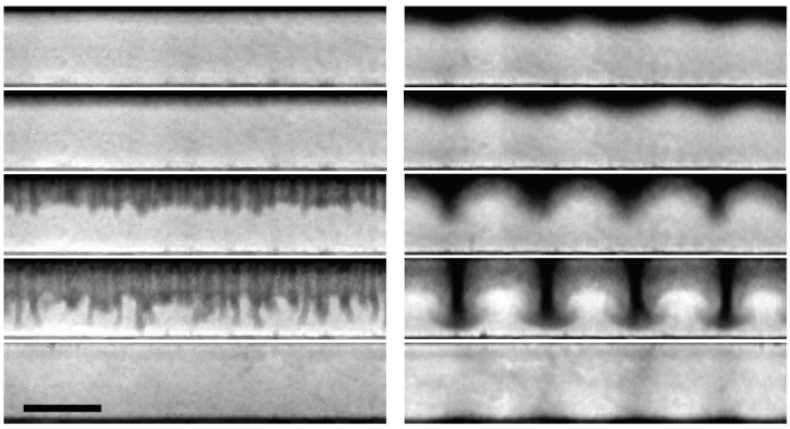

Figure 4.2: Time series of images of particle transport across the channel in response to a switch in the direction of the applied electric field, for $t_s = 1$ s (left) and $t_s = 5$ s (right). From top to bottom, the images are at times 0, 0.5, 1.0, 1.5, and 50 ms after the switch. Scale bar is 50 μm.

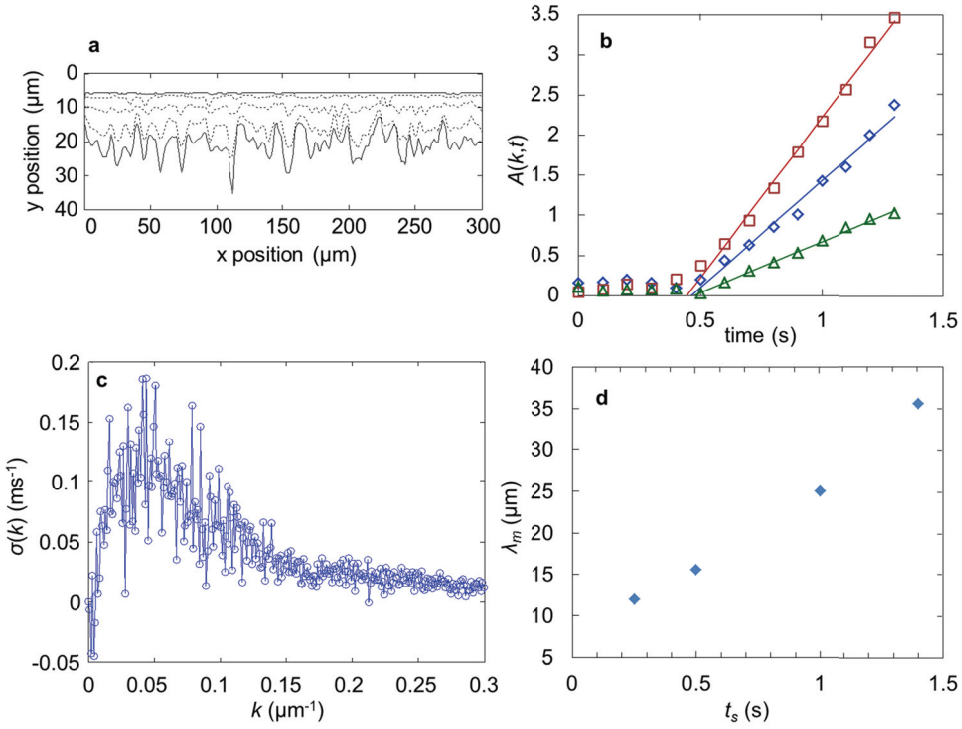

Figure 4.3: (a) Evolution of the profile of the particle front for a typical example where $t_s = 1$ s. The first trace, the nearly flat solid line, is taken at the moment the direction of the field is switched, at $t = 0$. The interval between each trace is 0.3 ms. (b) $A(k,t)$ vs. time for $k = .037$ (red squares), .030 (blue diamonds), and .076 μm^{-1} (green triangles); $t_s = 1$ s. The solid lines are linear fits. (c) Average growth rate vs. wavenumber for $t_s = 1$ s. (d) Fastest-growing wavelength for different t_s.

To analyze the fingering instability observed for $t_s = 1$ s, we use the images to track the time evolution of the particle front as it moves across the channel. By thresholding each image, we determine the profile of the front within the channel at different times, as shown in Figure 4.3(a). Each of the measured profiles can be represented by an ensemble of modes with different wavenumbers, k. By calculating the fast Fourier transform of each profile, we measure the amplitude

of each mode, $A(k,t)$, where t is time, and determine its temporal evolution. We find that immediately following the switch, there is little change in $A(k,t)$; however, approximately 0.5 ms after the switch, $A(k,t)$ grows linearly, as shown in Figure 4.3(b). Within the timeframe of linear growth, we linearly fit the time-dependence of $A(k,t)$ to $A(k,t) = \sigma(k)t$; we thereby obtain the growth rate, $\sigma(k)$, of every mode. The growth rate curve is broad, reflecting the growth of a wide range of modes. The fastest-growing mode, km, is approximately 0.04 μm^{-1}, as shown in Figure 4.3(c). This corresponds to a fastest-growing wavelength, λ_m, of $\lambda_m = k^{-1} = 25$ μm. We find that λ_m increases with t_s, for t_s between 0.25 and 1.4 s, as shown in Figure 4.3(d).

During the time between consecutive switches, after the particles have been transported completely across the channel and packed at the wall, they appear to diffuse, as shown in Figure 4.4(a). Thus, increasing the time between switches also increases the thickness of the particle-rich region at the beginning of each switch. We determine this thickness, l, by measuring the distance between the wall and the boundary between the particle-rich region and the particle-free fluid as a function of time following a switch in the direction of the applied field. Between 0.1 and 30 s after a switch, the growth of l is nearly diffusive, scaling as $t_s^{.42}$, as shown in Figure 4.4(b).

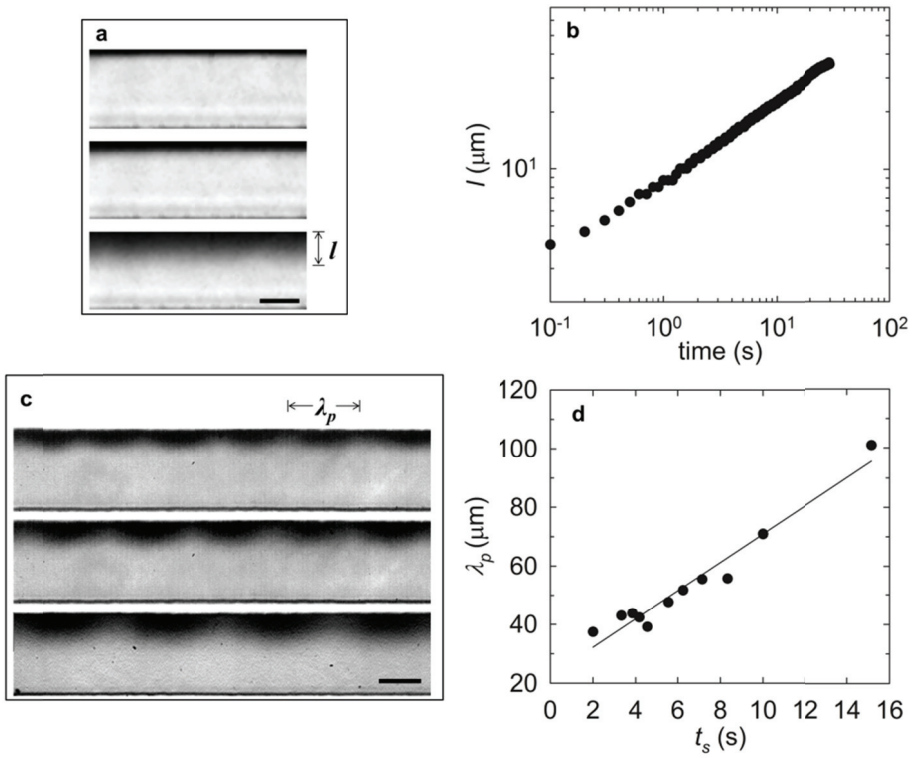

Figure 4.4: (a) Images of the channel after the particles are packed at the wall by a switch in the applied field at times 0.5 (top), 2 (middle), and 10 s (bottom) after the switch. Scale bar is 25 μm. (b) Thickness of particle-rich region vs. time; the field is switched at time = 0. (c) Images of the channel after many switches, for t_s = 3.33 (top), 5 (middle), and 10 s (bottom). The particles have formed a pattern at the wall. Scale bar is 25 μm. (d) Average characteristic wavelength of the pattern vs. time between consecutive switches. The solid line is a linear guideline.

Particle diffusion is critical in determining whether the particles are homogeneously distributed at the wall between switches or are localized in the well-defined pattern that is observed for t_s = 5 s. The fastest-growing fingers during particle transport reach the wall first; at this point, particles begin to deposit on the wall. This suggests that particles are deposited in higher amounts

at locations corresponding to the fastest-growing fingers. At lower t_s, where λ_m is smaller, the distance between neighboring fingers is small; therefore, the distance between areas of higher deposition is also small. Following deposition, diffusion transverse to the wall washes out the small inhomogeneities in the distribution of particles along the wall. Thus, by the next switch, and for all subsequent switches, the particle distribution in the particle-rich region remains uniform. By contrast, at higher t_s, for example $t_s = 5$ s, λ_m is larger; this results in a more heterogeneous deposition of particles at the wall. The distance between local peaks in particle concentration is now too large for diffusion to wash out these inhomogeneities before the field is switched again. Thus, the distribution of particles along the wall is non-uniform for the next switch. These areas of higher particle concentration form larger fingers during particle transport; moreover, they absorb smaller fingers that form nearby. This process repeats for subsequent switches, with each switch further reinforcing the localization of particles in these larger fingers. Eventually, the system reaches a steady state in which the particles are in a well-defined pattern along the wall and form thick, periodically-spaced fingers which resemble plumes during transport across the channel, as seen in the right panel of Figure 4.2. We observe the pattern formation for t_s

greater than 2 s; below this critical time, the particle distribution at the wall remains homogeneous between switches.

The pattern consists of a heterogeneous distribution of particles along the wall in which the areas of higher particle concentration are periodically spaced. Thus, the pattern has a characteristic wavelength, λ_p, which we measure as the average distance between peaks in the particle distribution. Because the pattern forms from the fastest-growing fingers, we expect λ_p to scale in the same way as λ_m. Indeed, we find that λ_p increases with the amount of time between switches, as shown in Figure 4.4(c); the growth of λ_p is approximately linear with t_s, as shown in Figure 4.4(d). For t_s greater than 16 s, the pattern no longer forms; at this point, t_s is sufficiently large enough such that particle diffusion completely washes out all non-uniformities in the particle-rich region.

The fingering instability during particle transport is reminiscent of the Rayleigh Taylor instability, which occurs for a system of two layers of fluid, where the denser fluid is above the less dense fluid; the interface between the fluids is unstable as gravity drives the heavier fluid downwards [21]. Similar behavior is observed for a colloidal suspension sedimenting through a fluid [22]. In our system, the positively-charged particles are in a stable configuration when they are packed against the wall adjacent to the negative electrode by the

applied field. When the direction of the field is switched, the system indeed becomes unstable, as the particles must move through the particle-free fluid to reach their new stable state at the opposite wall. This is analogous to the sedimentation of colloids through a fluid, suggesting that the behavior of our system can be described by similar physics and also exhibits the Rayleigh-Taylor instability. At early times of the Rayleigh-Taylor instability, perturbations in the interface between the fluids are described by a linear stability criterion and are expected to grow exponentially in time; the linear stability regime is valid only when the amplitudes of the perturbations are much smaller than their wavelengths. However, in the timeframe in which we observe our instability, the amplitudes of the fingers are large compared to their wavelengths; moreover, we measure the temporal growth of the modes to be linear, not exponential. Therefore, our instability has progressed beyond the linear to the nonlinear stability regime. Within the nonlinear regime of the Rayleigh-Taylor instability, the lengthscale of the fingers scales with the initial thickness of the unstable layer [23]. Indeed, we find that in our system, both the fastest-growing wavelength of the fingers and the thickness of the unstable particle layer increase with the time between consecutive switches. Thus, similar to the nonlinear Rayleigh Taylor

instability, an increase in the thickness of the particle layer corresponds to an increase in the fastest-growing wavelength of fingers during particle transport.

4.4 Conclusion

Here, we have visualized the dynamics of charged particles suspended in a nonpolar solvent in response to an applied electric field. We find that repeated switches in the direction of the applied field results in the localization of particles into a well-defined, periodic pattern whose characteristic wavelength is dependent on the frequency of the field. The pattern is due to a fingering instability which occurs as the particles are transported across the channel. This fingering instability can be compared to the Rayleigh-Taylor instability; however, determining the origin of the field-driven fingering instability and the mechanism for the fastest-growing modes requires further study. Our findings provide a basis for explaining the origin of patterns in electric-field-driven particle suspensions and for developing methods to reduce unwanted behaviors in electrophoretic displays, which is essential for the continued improvement of display technology.

References

[1] Q. Guo, V. Singh and S. H. Behrens, Langmuir, 2010, 26, 3203.

[2] I. D. Morrison, Colloids Surf. A, 1993, 71, 1.

[3] M. F. Hsu, E. R. Dufresne and D. A. Weitz, Langmuir, 2005, 21, 4881.

[4] S. K. Sainis, J. W. Merrill and E. R. Dufresne, Langmuir, 2008, 24, 13334.

[5] C. E. Espinosa, Q. Guo, V. Singh and S. H. Behrens, Langmuir, 2010, 26, 16941.

[6] Q. Guo, J. Lee, V. Singh and S. H. Behrens, J. Colloid Interface Sci., 2013, 392, 83.

[7] G. S. Roberts, R. Sanchez, R. Kemp, T. Wood and P. Bartlett, Langmuir, 2008, 24, 6530.

[8] G. N. Smith and J. Eastoe, Phys. Chem. Chem. Phys., 2013, 15, 424.

[9] S. M. Hashmi and A. Firoozabadi, Soft Matter, 2012, 8, 1878.

[10] J. W. Merrill, S. K. Sainis and E. R. Dufresne, Phys. Rev. Lett., 2009, 103, 138301.

[11] K. E. Tettey, M. Q. Yee and D. Lee, Langmuir, 2010, 26, 9974.

[12] V. Novotny, Colloids and Surfaces, 1987, 24, 361.

[13] B. Comiskey, J. D. Albert, H. Yoshizawa and J. Jacobson, Nature, 1998, 394, 253.

[14] P. Murau and B. Singer, J. Appl. Phys., 1978, 49, 4820.

[15] M. Trau et al., Nature (London), 1995, 374, 437.

[16] S.-R. Yeh, M. Seul and B. I. Shraiman, Nature (London), 1997, 386, 57.

[17] M. Trau, D. A. Saville and I. A. Aksay, Science, 1996, 272, 706.

[18] J. H. Kim et al., Langmuir, 2005, 21, 10941.

[19] D. Bartolo, G. Degre, P. Nghe and V. Studer, Lab Chip, 2007, 8, 274.

[20] T. Lin, T. E. Kodger and D. A. Weitz, Soft Matter, 2013, 9, 5173.

[21] D. Sharp, Physica (Amsterdam), 1984, 12D, 3.

[22] A. Wysocki et al., Soft Matter, 2009, 5, 1340.

[23] L. A. Newhouse and C. Pozrikidis, J. Fluid Mech., 1990, 217, 615.

Chapter 5

Conclusions

Here, we have presented an investigation of the dynamics of charged colloidal particles in nonpolar solvents. We find that the presence of reverse micelles has a significant effect on the transport of charged colloids as they move across a microfluidic channel. Because charged reverse micelles have a higher electrophoretic mobility than the particles, they move faster in a constant applied electric field; they arrive at the channel walls faster and screen the applied field, resulting in the decay of particle motion despite the continued application of the constant field. Furthermore, we find that at fields large enough to transport the particles completely across the channel, the particles do not transport homogeneously; instead, the rapidly advancing particle front develops a fingering instability. After the particles arrive at the channel wall, they appear to diffuse

freely away from the wall; this is also despite the continued application of the electric field. Repeated switches in the applied field results in the formation of a well-defined pattern; this pattern is dependent on the frequency of the applied field.

These results have significant implications for practical applications, especially electrophoretic displays, in which the ink is composed of charged pigment particles suspended in a nonpolar solvent. Charge control in these electronic inks is commonly achieved through the addition of surfactants which form reverse micelles. Reducing the amount of surfactant would reduce the effect of screening on the motion of the charged particles. However, if the amount of surfactant is decreased by too much, stabilization and control over the charge is lost. Furthermore, the motion of the particles depends on whether or not the applied field is switched or whether it is turned on or off; this must be taken into account to precisely control the trajectories of the particles. To overcome the screening effect altogether, the applied field can be increased; however, larger fields require more energy and may also introduce unwanted electrohydrodynamic effects. To change the image on the electrophoretic display, the applied field is frequently switched; this may lead to the formation of patterns. Additionally, special care must be taken to ensure that the particles do not freely diffuse back into the bulk

after they have been arranged in the desired configuration, as this degrades the quality of the image.

We have developed a method for directly visualizing charged particle suspensions in nonpolar solvents when they move in response to an applied electric field. We fabricate and use a microfluidic device that is resistant to swelling by organic solvents. The geometry of the microfluidic device can be easily redesigned. Additionally, the device provides a straightforward way of introducing fluid flow into the system. These features provide flexibility for further techniques to study charged particle suspensions. With this device, the full details of particle motion can be elucidated with high-speed imaging. Alternatively, we can observe and track individual particles within the device by using a confocal microscope.

The device provides a useful tool for investigating nonpolar systems. We are able to use a full range of particle concentrations, surfactant concentrations, and applied fields. This is a major advantage over the various equipment that are typically used to measure electrical properties in nonpolar media, as these equipment often have limitations regarding the properties of the particle suspension or the applied field. For example, we are able to visualize the motion of particles at relatively high volume fractions; at these concentrations,

hydrodynamic effects play a major role. Thus, we can investigate the onset of electrohydrodynamic effects and instabilities.

Our results also have implications in further studies of charging properties. By directly visualizing particle motion, we can capture the particle trajectories and use these trajectories to analyze the electrical properties of the suspension. At low volume fraction, the charged particles do not contribute significantly to the overall charge content of the suspension. The motion of the particles correlates directly with the internal field within the microfluidic channel. Thus, the charged particles serve as a direct probe of the internal field; we can detect spatial and temporal inhomogeneities in the local field within the channel. Additionally, we can use visualization to measure the electrophoretic mobility of the particles. However, because of the screening effect by the reverse micelles, the measured mobility is affected by the field that is induced by the reverse micelles. Thus, this measurement must be adjusted to find the actual mobility. Our device enables straightforward studies of the field-dependence of these various electrical properties.

In conclusion, we use direct visualization to investigate the behavior of charged particles in nonpolar solvents in response to an applied electric field. Our results are of significant relevance to practical applications, particularly

electrophoretic displays. Additionally, our findings further the understanding of the dynamics of charged colloids in nonpolar solvents.